Oil Shale, 2016, Vol. 33, No. 2, pp. 142–166
doi: 10.3176/oil.2016.2.04
ISSN 0208-189X

MULTIPLE CONTROLLING FACTORS OF THE ENRICHMENT OF ORGANIC MATTER IN THE UPPER CRETACEOUS OIL SHALE SEQUENCES OF THE SONGLIAO BASIN, NE CHINA: IMPLICATIONS FROM GEOCHEMICAL ANALYSES

YU SONG[(a,b)], ZHAOJUN LIU[(a,b)*], QINGTAO MENG[(a,b)], JINJUN XU[(a,b)], PINGCHANG SUN[(a,b)], LIJUAN CHENG[(c)], GUODONG ZHENG[(a,b)]

[(a)] College of Earth Sciences, Jilin University, Changchun 130061, China
[(b)] Key Laboratory for Oil Shale and Paragenetic Energy Minerals, Jilin University, Changchun 130061, China
[(c)] Institute of Geology and Geophysics, Chinese Academy of Sciences, Beijing 100029, China

Abstract. *Two oil shale sequences in the Upper Cretaceous Qingshankou and Nenjiang Formations of the Songliao Basin, NE China, representing organic matter (OM)-rich hydrocarbon source rocks, are investigated. According to bulk and inorganic geochemical data, there are significant differences in OM enrichment conditions between the first member of the Qingshankou Formation (K_2qn_1) and the second member of the Nenjiang Formation (K_2n_2). The oil shale in K_2qn_1 was deposited in a warm-humid paleoclimate, with strong water salinity stratification and dysoxic conditions, combined with high bioproductivity and low detrital matter input. In contrast, the oil shale in K_2n_2 was accumulated in a warm semi-humid paleoclimate, with weak water salinity stratification and partially oxic conditions, when the bioproductivity and detrital matter input were medium. In addition, the origin of OM influenced its enrichment. In summary, high bioproductivity and strong water salinity stratification were the major controlling factors for OM enrichment in K_2qn_1, while the origin of OM and dysoxic conditions were the major governing factors for OM enrichment in K_2n_2. Thus, the OM enrichment models of these two members are established.*

Keywords: *organic matter, enrichment conditions, oil shale sequences, Upper Cretaceous, Songliao Basin.*

* Corresponding author: e-mail *liuzj@jlu.edu.cn*

1. Introduction

Sedimentary organic matter (OM) enrichment is controlled by several factors, including biological productivity, continental weathering, sedimentation rate, clay mineralogy, redox conditions, sea level change, and sedimentary environment [1–3]. However, the three primary mechanisms controlling OM enrichment are input, preservation and dilution of OM [4–6]. The input to OM is mainly controlled by primary productivity [7–9], the preservation of OM is related to redox conditions and water salinity [10, 11], whereas the dilution of OM is associated with detrital matter input [12, 13].

The Songliao Basin has attracted widespread attention in recent years due to the development of oil shale sequences K_2qn_1, K_2n_1 and K_2n_2 in the Upper Cretaceous [14–17]. Beside their commercial value, the sequences provide valuable information about OM enrichment. The Songliao Basin is the largest Cretaceous lacustrine rift basin located in NE China. The depositional environments in different basin regions are dissimilar, especially the northern and southern parts of the basin have been influenced by different sedimentary systems (Fig. 1) [18]. Previous studies about the Upper Cretaceous oil shale sequences mainly focused on the southeastern part of

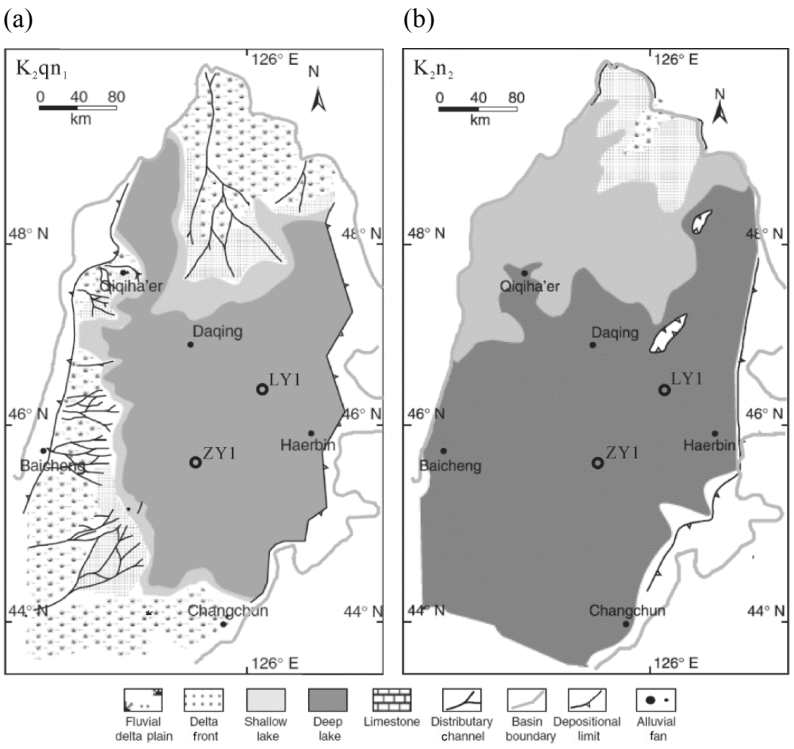

Fig. 1. Areal distribution of sedimentary facies within the Songliao Basin during deposition of (a) K_2qn_1 and (b) K_2n_2 (modified after [18]).

the Songliao Basin [14–16], whereas investigations about OM accumulation conditions in the basin's northern part are relatively few. In this study, the influencing factors such as bioproductivity, preservation and dilution of OM in K_2qn_1 and K_2n_2 oil shale sequences are discussed, based on the abundant bulk and inorganic geochemical data from two sampled core profiles located in the northern part of the Songliao Basin, in order to reveal the different enrichment mechanisms of two oil shale sequences and establish their OM enrichment model.

2. Regional geological setting

Based on the Mesozoic tectonic evolution, combined with the basement structure and caprock development characteristics, the Songliao Basin is divided into six first-order structural units as follows: the Northern Plunge, the Northeastern Uplift, the Southeastern Uplift, the Central Downwarp, the Western Slope and the Southwestern Uplift (Fig. 2) [18]. The basin evolution can be subdivided into pre-rift doming, syn-rift subsidence, post-rift thermal subsidence, and structural inversion stages (Fig. 3) [19].

The Songliao Basin contains clastic deposits of Jurassic to Cenozoic age, which are more than 10 km thick. The basin fill thins toward the basin margins and is dominated by Cretaceous terrigenous successions [18].

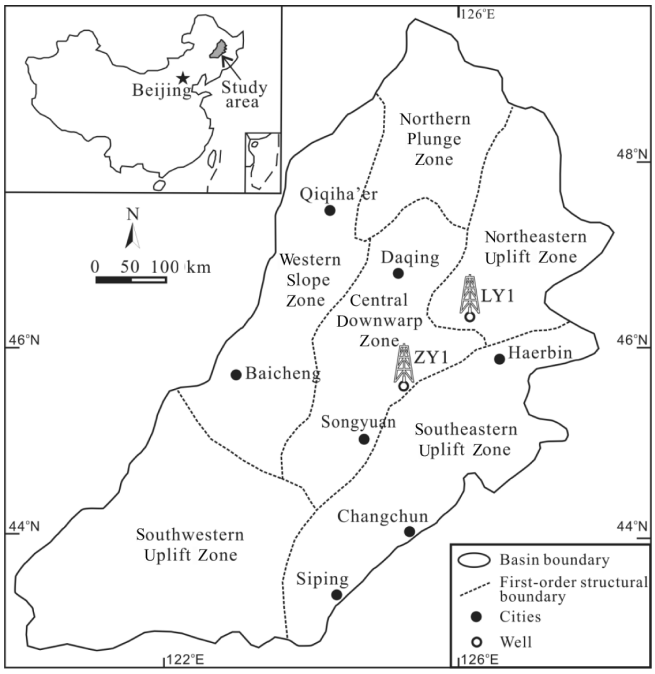

Fig. 2. Location map showing the Songliao Basin and its structural units. Shown are the locations of wells (modified after [15]).

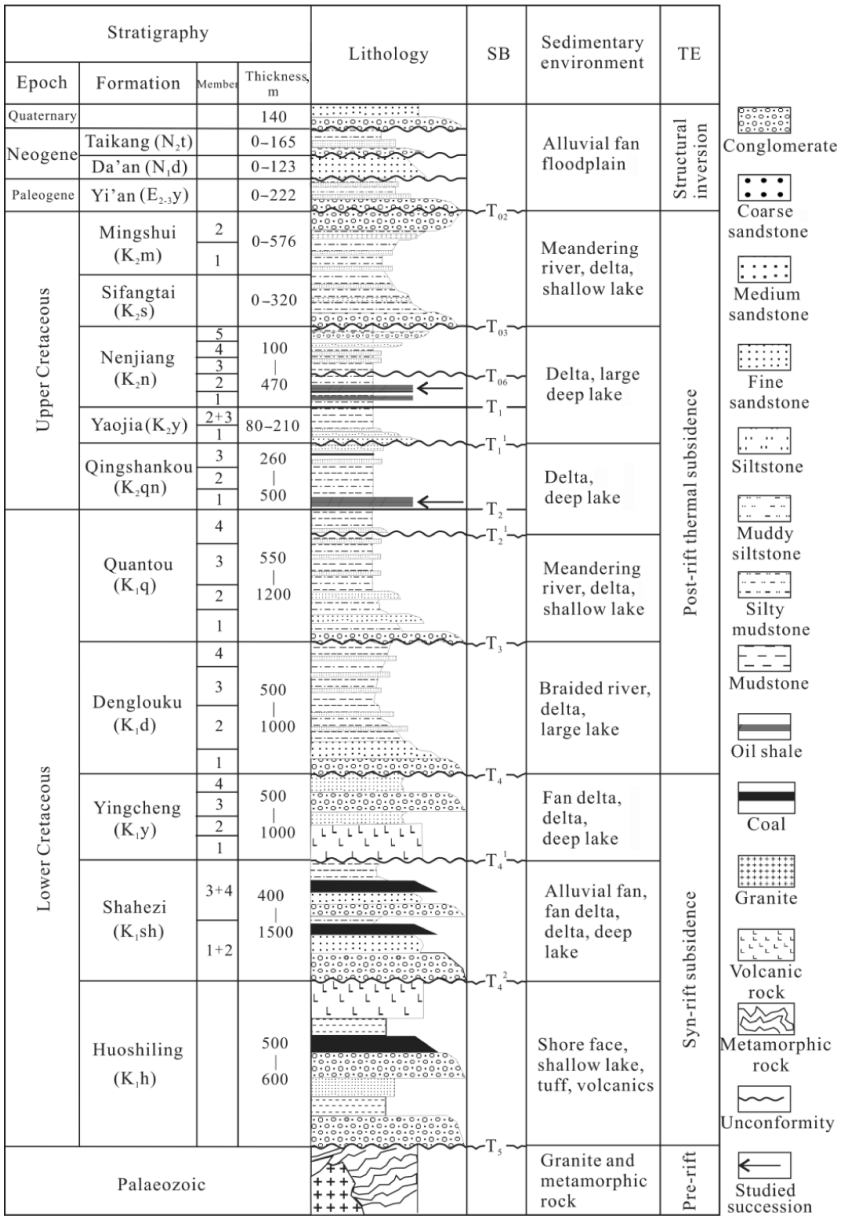

Fig. 3. Generalized stratigraphic column (modified after [18]).

The Upper Cretaceous Qingshankou and Nenjiang Formations are the main hydrocarbon source rocks (Fig. 3). Based on lithology, the Qingshankou Formation is subdivided into three members (K_2qn_1, K_2qn_2 and $K_2qn_{3)}$. The oil shale succession occurs in the lowermost Member 1 (K_2qn_1). It developed during a period characterized by semi-deep to deep lake facies, the lake area being 8.7×10^4 km^2 (Fig. 1a) [18]. The sediments are composed of dark grey to grey/grey-black mudstone, grey-brown/brown oil shale (Fig. 4c–d), and

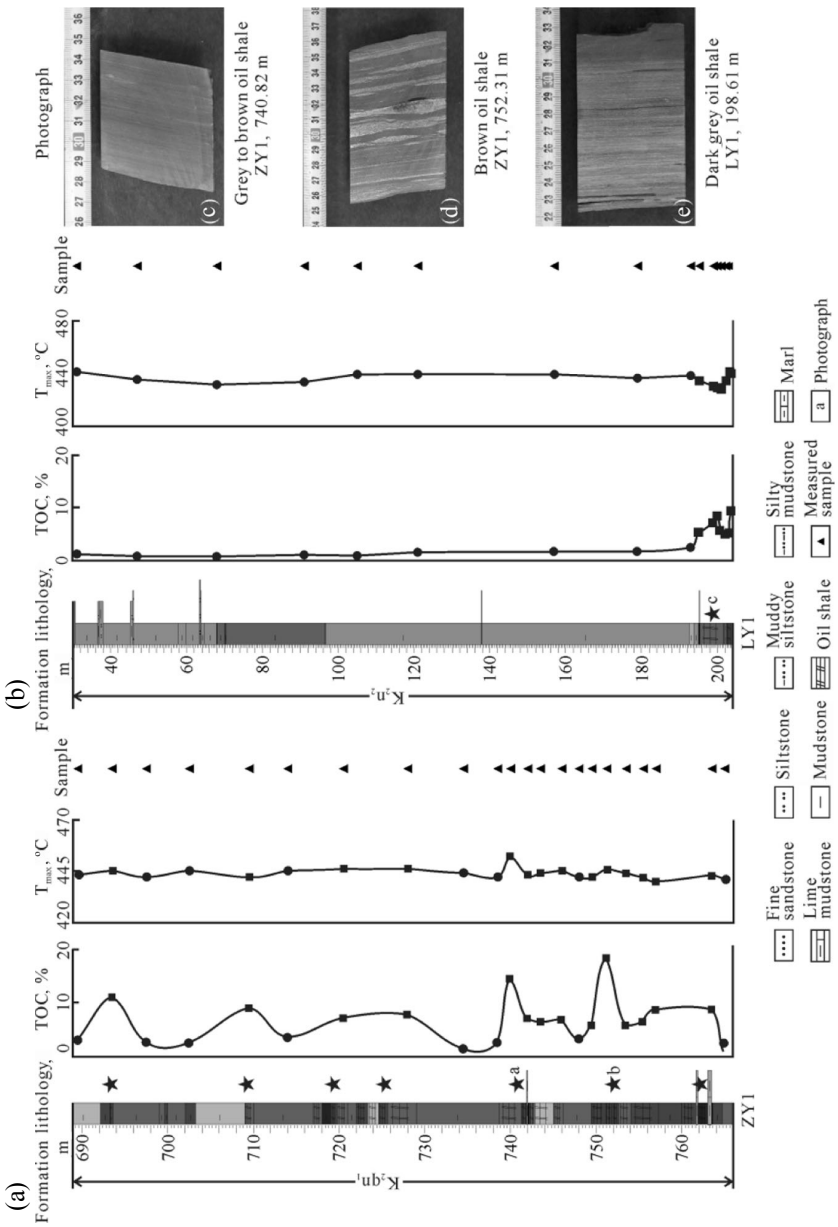

Fig. 4. Lithologic profile with the position of measured samples from wells ZY1 (a) and LY1 (b); shown are the photographs of borehole cores ((c)–(e)).

yellow-grey marl. According to lithology, the Nenjiang Formation is subdivided into five members (K_2n_1, K_2n_2, K_2n_3, K_2n_4 and K_2n_5). Near the base of Member 2 there developed a 7 m thick excellent oil shale. During the deposition of Member 2, a semi-deep to deep lake facies developed in the basin, covering an area of 20×10^4 km^2 (Fig. 1b) [18]. The sediments are composed of (dark) grey mudstone and dark grey/grey-black oil shale (Fig. 4e).

3. Sampling and methods

Samples for the study were collected from wells ZY1 and LY1. Well ZY1 is located in the Central Downwarp Zone, the K_2qn_1 samples were taken at a depth from 689 to 769.66 m. Well LY1 is located in the Northeastern Uplift Zone and the K_2n_2 samples were taken at a depth from 30 to 204 m (Fig. 2). Most of the samples were dark grey or grey-brown oil shale, or dark grey to grey mudstone. 38 samples from K_2qn_1 and K_2n_2 were subjected to elemental (C, S), Rock-Eval, major element oxides and trace elements analyses (Fig. 4a–b).

The elemental (C, S) and Rock-Eval analyses were carried out at the Key Laboratory for Oil Shale and Paragenetic Energy Minerals, Changchun, China. The total organic carbon (TOC) was measured by the Leco CS-230 instrument on samples pretreated with concentrated HCl. The total sulfur (S) contents were determined with the same instrument. Pyrolysis was carried out using the Rock-Eval 6 standard instrument. The Rock-Eval method estimates the amount of pyrolyzate (mg HC/g rock) that is released from kerogen during gradual heating in a He stream and normalized to the TOC content gives the hydrogen index (HI). The temperature of maximum generation (T_{max}) serves as a maturation indicator. The samples were analyzed for major element oxides and trace elements at the Beijing Research Institute of Uranium Geology, China, using a Philips PW2404 X-ray fluorescence (XRF) spectrometer and a high resolution inductively coupled plasma mass spectrometer (HR-ICP-MS; Thermo Scientific X-Series) and following the criteria of Chinese national standards GB/T 14506.28-93 and DZ/T 0223-2001, respectively.

4. Characteristics of organic matter and accumulation conditions

4.1. Bulk geochemistry

The total organic carbon (TOC) content in the K_2qn_1 oil shale varies between 5.76 and 14.4 wt% (avg. 8.79 wt%), in mudstone from 1.04 to 3.67 wt% (avg. 2.56 wt%). All these values are higher than the respective figures in the K_2n_2 oil shale (5.19–9.44 wt%, avg. 6.66) and mudstone (0.85–2.55 wt%, avg. 1.44 wt%) (Fig. 4, Table). The Rock-Eval T_{max} of oil shale and mudstone from both members is 429–452 °C, indicating that these rocks are

immature to marginally mature (Fig. 4, Table) [20], which is equivalent to a vitrinite reflectance (Ro) of about 0.5% Ro [16].

Table. The elemental abundances and the correponding ratios in the samples from K_2qn_1 and K_2n_2

Sample No	Depth, m	Lithology	TOC[a], wt%	TS[b], %	Fe, %	T_{max}, °C	HI[c], mg HC/g TOC	Al_2O_3/TiO_2
1st member of Qingshankou Formation								
Z1	689.5	Dark grey mudstone	3.13	0.97	2.20	443	691.78	36
Z2	693.5	Grey-brown oil shale	10.90	1.17	2.46	445	726.24	29
Z3	697.5	Dark grey mudstone	2.77	0.75	3.12	442	681.87	28
Z4	702.5	Grey-black mustone	2.58	0.81	4.10	445	675.52	27
Z5	709.5	Grey-brown oil shale	9.01	0.88	2.55	442	792.34	28
Z6	714	Dark grey mudstone	3.67	0.78	3.33	445	703.01	28
Z7	720.5	Dark grey oil shale	7.18	1.26	2.87	446	826.04	30
Z8	728	Dark grey oil shale	7.78	0.75	2.82	446	737.36	28
Z9	734.5	Grey-black mudstone	1.49	0.90	3.21	444	583.71	27
Z10	738.5	Dark grey mudstone	2.59	0.63	3.63	442	675.87	27
Z11	740	Grey-brown oil shale	14.40	0.85	3.51	452	730.28	28
Z12	742	Grey-brown oil shale	7.07	1.43	3.23	443	362.09	29
Z13	743.5	Grey-brown oil shale	6.39	0.82	2.94	444	805.01	29
Z14	746	Grey-brown oil shale	6.75	0.48	3.03	445	789.33	30
Z15	748	Dark grey mudstone	3.23	0.50	3.39	442	706.81	28
Z16	749.5	Grey oil shale	5.76	0.41	2.87	442	554.17	27
Z17	751.3	Grey-black oil shale	18.25	1.30	2.26	446	752.82	28
Z18	753.5	Dark grey oil shale	5.81	0.86	3.07	444	766.06	29
Z19	755.5	Grey-black oil shale	6.39	0.82	3.15	442	469.33	28
Z20	757	Grey oil shale	8.66	0.82	3.62	440	735.80	27
Z21	763.5	Grey-black oil shale	8.68	1.16	2.18	443	740.51	20
Z22	765	Dark grey mudstone	1.04	1.60	2.74	441	379.81	24
2nd member of Nenjiang Formation								
L1	31	Grey mudstone	1.24	0.11	2.78	442	42.74	22
L2	47	Grey mudstone	0.96	0.17	2.97	436	93.65	23
L3	68	Grey-black mudstone	0.85	0.05	2.72	432	44.65	23
L4	91	Dark grey mudstone	1.18	0.15	4.53	434	79.66	25
L5	105	Grey mudstone	1.04	0.16	9.77	440	106.73	24
L6	121	Grey mudstone	1.64	0.22	4.00	440	80.73	23
L7	157	Grey mudstone	1.72	0.31	3.36	440	91.55	22
L8	179	Grey mudstone	1.81	0.29	3.05	437	163.43	22
L9	193	Grey-brown mudstone	2.55	0.57	1.58	439	357.96	27
L10	195.23	Grey oil shale	5.31	0.61	2.21	435	733.72	27
L11	199	Dark grey oil shale	7.14	1.34	2.69	431	759.80	23
L12	200	Grey-brown oil shale	8.49	1.37	2.26	430	771.86	24
L13	201	Grey-black oil shale	5.75	0.65	2.13	429	741.51	25
L14	202.23	Grey-brown oil shale	5.19	0.43	3.76	435	731.47	23
L15	203.25	Grey-black oil shale	5.29	0.78	2.92	442	733.34	22
L16	203.75	Grey-black oil shale	9.44	1.42	2.78	441	778.22	20

Table (continued)

Sample No	TOC, wt%	P, %	U, μg/g	Sr/Cu	EF[d]	V/Cr	δCe	Ti/Al	Si/Al	Sr/Ba	Ca/(Ca + Fe)
1st member of Qingshankou Formation											
Z1	3.13	0.041	4.29	12.61	6.04	2.36	–0.043	0.0318	2.69	0.86	0.63
Z2	10.90	0.123	9.55	11.54	5.98	2.91	0.145	0.0387	3.06	1.52	0.75
Z3	2.77	0.077	5.36	8.01	3.79	2.18	–0.073	0.0410	2.88	0.62	0.25
Z4	2.58	0.097	5.24	11.49	3.38	2.46	–0.070	0.0423	2.86	0.77	0.34
Z5	9.01	0.074	5.89	4.72	4.91	2.10	–0.048	0.0412	2.95	0.90	0.59
Z6	3.67	0.044	6.08	11.57	2.15	2.46	–0.057	0.0410	2.94	0.91	0.36
Z7	7.18	0.048	4.97	3.13	2.83	2.44	–0.081	0.0380	2.88	0.50	0.16
Z8	7.78	0.048	4.68	5.79	4.55	2.44	–0.030	0.0408	3.00	0.62	0.19
Z9	1.49	0.070	5.41	4.52	4.06	2.19	–0.045	0.0419	3.04	0.78	0.38
Z10	2.59	0.053	4.11	7.79	4.13	2.78	–0.034	0.0418	3.07	0.78	0.31
Z11	14.40	0.148	5.61	15.19	3.51	2.14	0.021	0.0401	3.17	1.70	0.66
Z12	7.07	0.075	3.43	11.80	1.57	2.02	–0.052	0.0386	2.89	0.26	0.33
Z13	6.39	0.120	8.37	6.68	5.16	2.44	–0.020	0.0390	2.94	0.80	0.33
Z14	6.75	0.258	9.15	8.04	4.86	2.15	–0.025	0.0374	3.02	1.09	0.44
Z15	3.23	0.112	6.65	3.91	3.25	2.25	–0.039	0.0412	2.90	0.75	0.20
Z16	5.76	0.070	3.83	13.04	1.22	2.20	–0.006	0.0423	2.92	1.15	0.56
Z17	18.25	0.254	7.99	4.41	4.49	2.96	0.040	0.0401	3.04	0.99	0.36
Z18	5.81	0.094	5.86	6.53	3.57	2.16	–0.055	0.0394	2.85	0.84	0.37
Z19	6.39	0.134	5.98	7.67	3.32	2.61	–0.030	0.0411	3.03	0.98	0.64
Z20	8.66	0.088	6.1	5.28	3.82	2.23	–0.059	0.0418	3.03	0.70	0.16
Z21	8.68	0.041	7	9.08	40.16	2.14	–0.020	0.0578	4.98	0.69	0.90
Z22	1.04	0.089	3.9	11.36	1.57	1.97	–0.036	0.0477	3.17	0.99	0.50
2nd member of Nenjiang Formation											
L1	1.24	0.045	2.81	4.97	0.28	1.42	–0.023	0.0510	3.26	0.32	0.21
L2	0.96	0.054	2.52	5.43	0.29	1.59	–0.025	0.0499	3.01	0.34	0.23
L3	0.85	0.060	2.66	4.72	0.24	1.51	–0.022	0.0486	2.76	0.34	0.26
L4	1.18	0.111	3.24	6.07	0.38	1.52	–0.013	0.0448	2.74	0.38	0.20
L5	1.04	0.190	2.29	6.54	0.26	2.14	–0.027	0.0477	2.83	0.39	0.17
L6	1.64	0.084	1.98	6.90	0.34	1.19	–0.064	0.0492	3.16	0.43	0.15
L7	1.72	0.052	2.59	5.57	0.45	1.12	–0.029	0.0517	3.41	0.41	0.13
L8	1.81	0.100	2.88	5.52	0.57	1.40	–0.021	0.0512	3.62	0.40	0.20
L9	2.55	0.035	5.99	5.86	2.45	2.13	0.017	0.0421	5.67	0.91	0.20
L10	5.31	0.040	4.24	3.09	2.65	1.58	–0.045	0.0422	4.96	0.38	0.13
L11	7.14	0.124	6.7	3.27	5.00	2.02	–0.059	0.0495	4.49	0.46	0.48
L12	8.49	0.092	6.15	2.79	3.97	2.19	–0.061	0.0467	5.30	0.35	0.18
L13	5.75	0.073	4.61	3.48	2.12	1.74	–0.048	0.0456	4.64	0.36	0.26
L14	5.19	0.059	4.69	3.04	2.37	1.88	–0.069	0.0483	3.87	0.28	0.21
L15	5.29	0.052	5.78	3.15	1.76	1.73	–0.067	0.0519	3.70	0.35	0.24
L16	9.44	0.064	9.25	2.27	4.24	1.59	–0.035	0.0562	3.80	0.33	0.18

[a] stands for total organic carbon, [b] stands for total sulfur, [c] stands for hydrogen index, [d] stands for $EF_{Mo/Al}$.

4.2. Sediment provenance

During the period of accumulation of the Qingshankou and Nenjiang Formations in the Songliao Basin, the Al_2O_3/TiO_2 ratio was 20–36 and 20–27, respectively. This ratio is a useful indicator of sedimentary rocks origin, which implies a constant sediment source region from intermediate to felsic igneous rocks [21]. In addition, a good correlation between the contents of Al_2O_3 and TiO_2 (Fig. 5) indicates either the occurrence of titanium (Ti) within clay lattices or that the detrital material came from a constant source, suppressing the effect of winnowing processes [22].

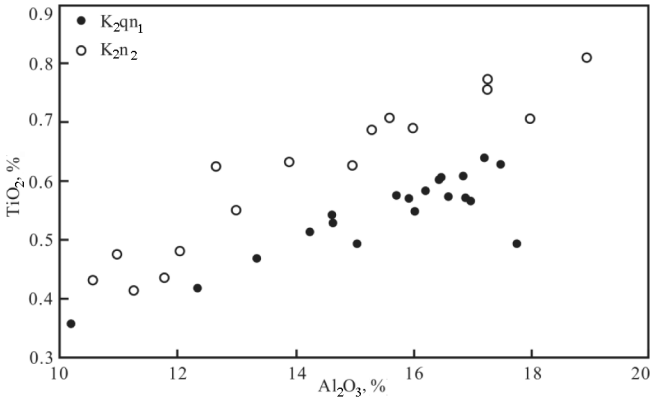

Fig. 5. The diagram of Al_2O_3 and TiO_2 contents of the samples of K_2qn_1 and K_2n_2.

4.3. Paleoclimate

The strontium (Sr)/copper (Cu) ratio is an important elemental indicator of paleoclimate reconstruction, generally Sr/Cu ratios between 1.3 and 5.0 suggest a warm-humid climate, whereas a ratio > 5.0 points to a hot-arid climate [23]. However, the concentrations of Sr and Cu have been influenced by the extent of the lake basin, offshore distance, and water depth [15]. But, generally, the high Sr/Cu ratio reflects the hot-arid paleoclimate, and the low Sr/Cu ratio implies the warm-humid paleoclimate.

According to Jia et al. [15], a Sr/Cu ratio of 10.0 was taken as the boundary for the climate division of K_2qn_1. The Sr/Cu ratio within K_2qn_1 varies between 3.13 and 13.04 (avg. 8.37) (Fig. 6, Table), indicating a warm-humid paleoclimate. According to Huang et al. [24], during the deposition of K_2qn_1, vegetation consisted of a coniferous and broadleaf mixed forest with some hassocks, pointing to a warm-humid southern subtropical paleoclimate. This interpretation is confirmed by oxygen isotope data [25].

The Sr/Cu ratio within K_2n_2 varies between 2.27 and 6.90 (avg. 4.54) (Fig. 7, Table), suggesting a warm semi-humid paleoclimate. The type of vegetation was a coniferous forest with some hassocks, implying a warm

semi-humid northern tropical paleoclimate [24], which is also supported by oxygen isotope data [25].

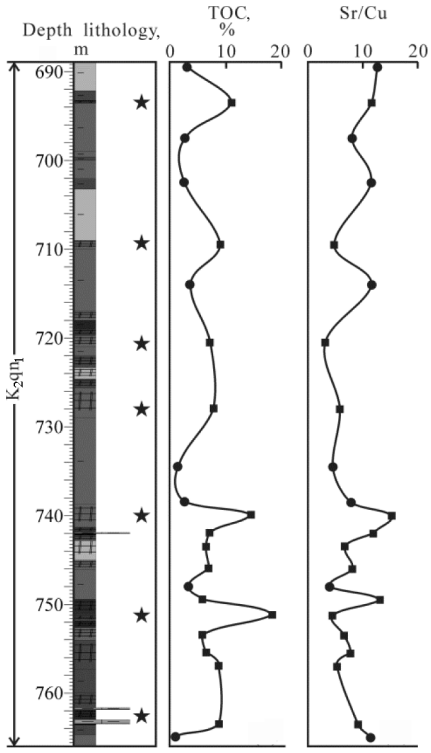

Fig. 6. The vertical variation of the paleoclimate proxy Sr/Cu ratio in K_2qn_1. ★ symbolizes oil shale layers, ■ denotes oil shale samples, ● stands for mudstone samples. TOC contents are shown for comparison.

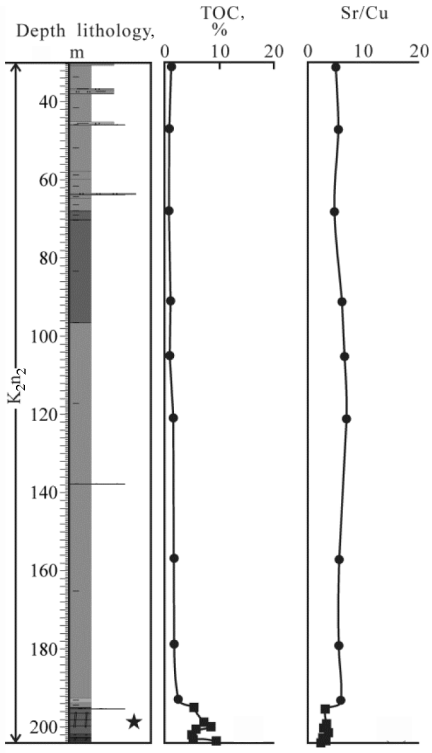

Fig. 7. The vertical variation of the paleoclimate proxy Sr/Cu ratio in K_2n_2. TOC contents are shown for comparison.

4.4. Paleo-redox conditions

4.4.1. C-S-Fe relationships

Within K_2qn_1, the average TOC in oil shale and mudstone is 8.79 and 2.56 wt%, respectively, which are higher than the respective figures in K_2n_2, 6.66 and 1.44 wt%. Based on the systematic analysis of K_2qn_1 and K_2n_2 samples, there is a very low contribution from inorganic carbon (generally < 0.8 wt%) [14, 15].

The total sulphur (TS) content in the K_2qn_1 oil shale varies between 0.41 and 1.43 wt% (avg. 0.93 wt%), being close to that in the K_2n_2 oil shale (0.43–1.42 wt%, avg. 0.94 wt%). At the same time, the TS content in the

mudstone of K_2qn_1 ranges from 0.50 to 1.60 wt% (avg. 0.87 wt%), which is much higher than the value in the K_2n_2 mudstone (0.05–0.57 wt%, avg. 0.23 wt%) (Table).

C-S crossplots have been used to differentiate oxic environments from euxinic. The sediments that accumulated under oxygenated conditions show a strong positive correlation between TOC and TS, and the trend line has a zero intercept. In contrast, the TOC vs TS plot of sediments formed in euxinic environments shows a nonzero sulphur intercept and may or may not reveal any correlation [26].

The plots of TOC vs TS demonstrate that there are distinct differences between K_2qn_1 and K_2n_2. For K_2qn_1, the corresponding plot shows no correlation ($r^2 = 0.05$) and a line fit through the data produces a positive intercept around 0.8 (Fig. 8a). In contrast, this plot for K_2n_2 illustrates a positive correlation ($r^2 = 0.90$) and an intercept that is close to zero (–0.03) (Fig. 8b). It indicates that K_2qn_1 may have accumulated under dysoxic or anoxic conditions, and K_2n_2 may have formed under oxic conditions.

Degree of pyritization (DOP) is the ratio of pyritic iron to total reactive iron (pyritic iron plus HCl-soluble iron), which can reflect redox conditions that prevailed during sediment accumulation. DOP values lower than 0.42 imply oxic conditions, and values higher than 0.75 reflect conditions with no oxygen available (anoxic) and possibly with H_2S available (euxinic). Values between 0.42 and 0.75 indicate dysoxic conditions [27].

Dean and Arthur [28] and Arthur and Sageman [29] suggested that ternary C-S-Fe diagrams could be used to approximate DOP. On this ternary diagram, the samples accumulated under oxygenated conditions plot along a line equivalent to a S/C ratio of 0.4; samples in which all of the iron (Fe) is reactive and fixed as pyritic sulphur plot along the line having a S/Fe ratio of 1.15 (based on the stoichiometry of pyrite).

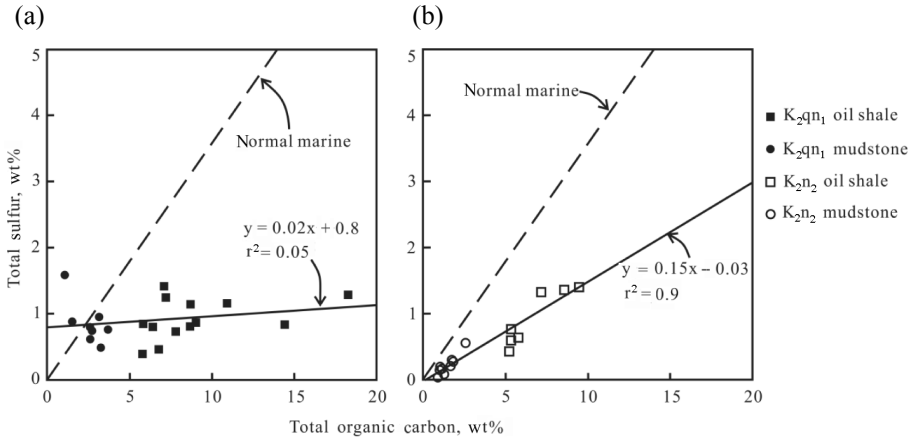

Fig. 8. Carbon-sulfur relationships of (a) K_2qn_1 and (b) K_2n_2. (Solid lines represent linear regression lines for data from this study; dashed lines show a typical S/C ratio for normal marine sediments, based on [26]).

The K_2qn_1 and K_2n_2 samples exhibit different C-S-Fe relationships (Fig. 9a and 9b, respectively). The oil shale and mudstone samples of K_2qn_1 plot along a line that intersects the Fe-S axis at approximately 0.3 (i.e. 30% S and 70% Fe) and 0.25, respectively (Fig. 9a). Thus, about 56% (or 0.3/0.54) and 46% of the iron is in pyrite, respectively. Based on these values, the DOPs of 0.56 (K_2qn_1 oil shale) and 0.46 (K_2qn_1 mudstone) are inferred, signifying the dysoxic environment, but the reducibility of oil shale is higher than that of mudstone.

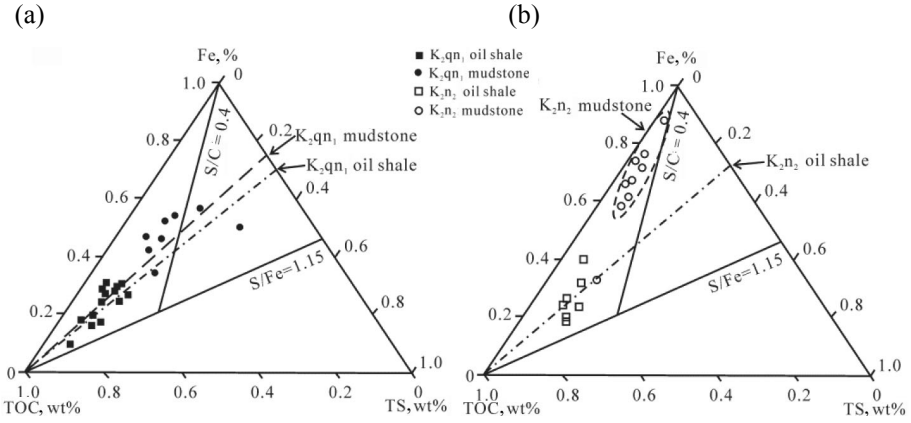

Fig. 9. C-S-Fe ternary diagrams of (a) K_2qn_1 and (b) K_2n_2.

The K_2n_2 oil shale samples plot along a line that intercepts the Fe-S axis around 0.28 (Fig. 9b), suggesting a DOP of approximately 0.52 that reflects dysoxic conditions. However, the K_2n_2 mudstone samples do not plot along the line of a constant S/Fe and tend to cluster around the S/C = 0.4 line, reflecting marginally oxic conditions. One mudstone sample plots along the "oil shale" line, indicating partially dysoxic conditions.

4.4.2. Hydrogen index

The hydrogen index (HI = $S_2 \times 100$/TOC) may reflect the type of redox conditions, generally a high HI points to reducing conditions, and a low value implies oxidizing conditions [30]. The high HI in oil shale and mudstone (avg. 699 and 637 mg HC/g TOC, respectively) argues for a strongly reducing environment during the deposition of K_2qn_1 (Fig. 10, Table). In contrast, the high HI value in oil shale (avg. 750 mg HC/g TOC) and the low one in mudstone (avg. 118 mg HC/g TOC) indicate at least limited oxygen availability during the sedimentation of K_2n_2 (Fig. 11, Table).

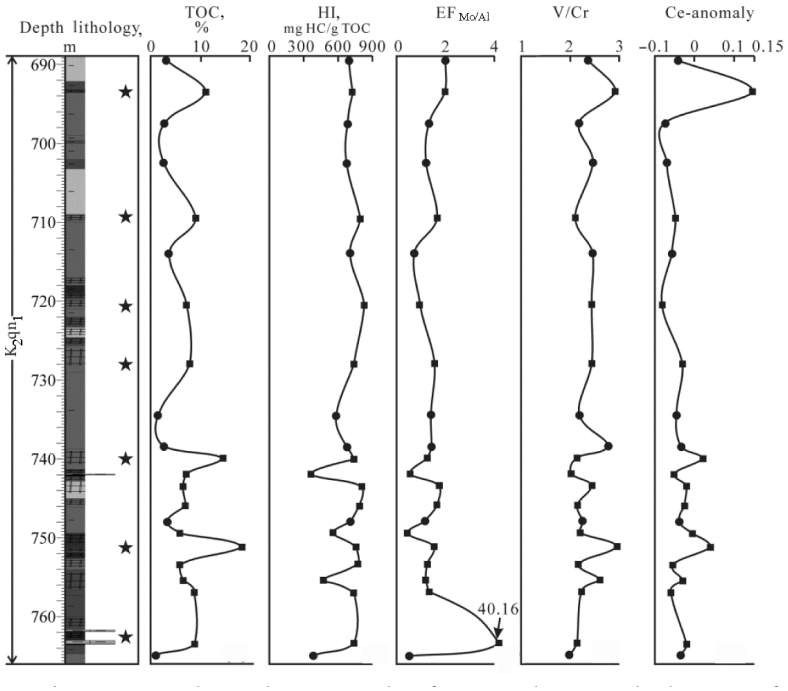

Fig. 10. Paleo-redox proxies HI, $EF_{Mo/Al}$, V/Cr and Ce-anomaly of trace and rare earth elements of K_2qn_1. TOC contents are shown for comparison.

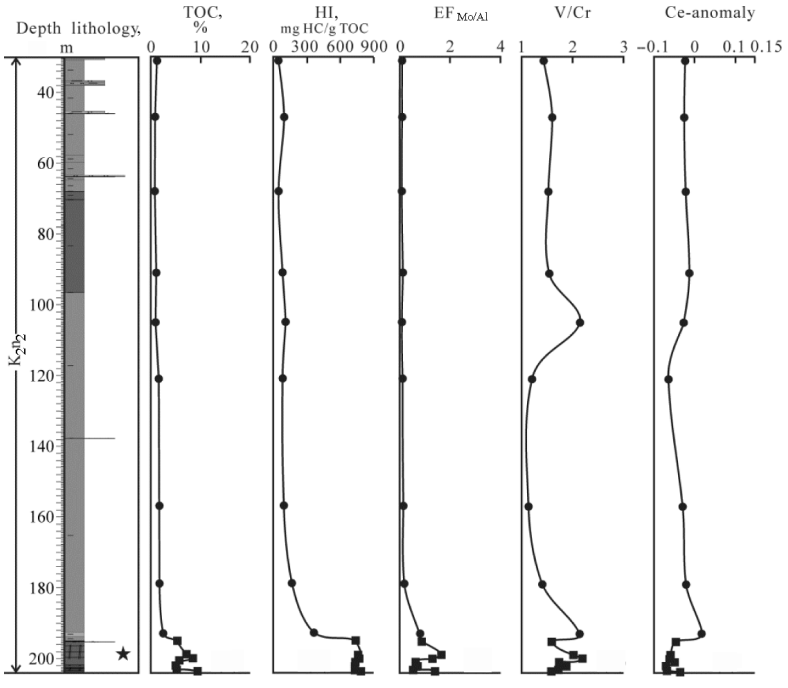

Fig. 11. Paleo-redox proxies HI, $EF_{Mo/Al}$, V/Cr, and Ce-anomaly of trace and rare earth elements of K_2n_2. TOC contents are shown for comparison.

4.4.3. Trace and rare earth elements

The molybdenum enrichment factor ($EF_{Mo/Al}$) is defined as $(Mo/Al)/(Mo/Al)_{shale}$, the ratio in the denominator being representative for a "typical" shale, using data from [31]. A high $EF_{Mo/Al}$ reflects anoxic conditions, and a low $EF_{Mo/Al}$ points to oxic conditions [32, 33]. The average $EF_{Mo/Al}$ of oil shale and mudstone within K_2qn_1 is 6.43 and 3.55, respectively (Fig. 10, Table), being higher than the corresponding figures in the K_2n_2 oil shale (avg. 3.16) and mudstone (avg. 0.58) (Fig. 11, Table).

Vanadium (V) is thought to occur in tetrapyrrole structures that are preserved preferentially under anoxic conditions. Chromium (Cr) is believed to be associated only with the detrital fraction, and is not influenced by redox conditions [34]. Thus, the low V/Cr ratio (0–2) indicates oxic conditions, the moderate ratio (2–4.25) implies dysoxic conditions, whereas the high ratio (> 4.25) points to anoxic conditions [34]. The V/Cr ratios in the K_2qn_1 oil shale and mudstone are from 2.02 to 2.96 (avg. 2.35) and 1.97–2.78 (avg. 2.33), respectively (Fig. 10, Table). However, the V/Cr ratios of K_2n_2 oil shale (1.58–2.19, avg. 1.82) and mudstone (1.12–2.14, avg.1.56) are much lower (Fig. 11, Table).

Cerium-anomaly (Ce-anomaly = log $[2Ce_n/(La_n + Pr_n)]$, the subscript "n" symbolizing the concentration normalized to chondrite) has been widely used to trace bottom water redox conditions. Generally, the high Ce-anomaly (> –0.10) indicates reducing conditions, whereas the low Ce-anomaly (< –0.10) points to oxidizing conditions [35]. The Ce-anomaly in the K_2qn_1 oil shale (–0.081 to –0.145, avg. –0.016) is higher than that in mudstone (–0.073 to –0.034, avg. –0.049) (Fig. 10, Table). However, the Ce-anomaly of K_2n_2 oil shale (–0.067 to –0.035, avg. –0.055) is lower than that in mudstone (–0.064 to –0.017, avg. –0.023) (Fig. 11, Table). It is possibly because in oxic conditions, Ce is less readily dissolved in water, so that oxic water is more depleted of Ce, whereas oxic sediments are more enriched in Ce [35].

The contents of the above trace and rare earth elements reveal that during the deposition of K_2qn_1 oil shale and mudstone, redox conditions prevailed, which is consistent with the proposition about the existence of dysoxic conditions. Whereas the K_2n_2 sediments were accumulated in fluctuant redox conditions, oil shale in the lower part of the Songliao Basin deposited in dysoxic conditions and mudstone in its upper part formed in marginally oxic conditions.

4.5. Terrigenous detrital matter input

As there are no significant differences in sediment provenance between K_2qn_1 and K_2n_2 (see 4.2), titanium (Ti) can be generally associated with terrestrial detritus and coarser grained sediments in high energy environments, and aluminium (Al) is abundant mainly in clay minerals. Thus, a higher Ti/Al ratio reflects an increased input of detrital matter [14, 22, 36].

The silicon (Si)/Al ratio has also been used as a proxy for detrital influx [8, 12].

The Ti/Al and Si/Al ratios in the K_2qn_1 oil shale (avg. 0.0412 and 3.13, respectively) are slightly higher than those in mudstone (avg. 0.0411 and 2.94, respectively) (Fig. 12, Table). Within K_2n_2 these ratios are relatively high, being somewhat higher in oil shale (avg. 0.0486 and 4.39, respectively) compared with mudstone (avg. 0.0485 and 3.38, respectively) (Fig. 13, Table).

The data show that the detrital input during the deposition of K_2qn_1 was low, and during the deposition of K_2n_2 moderate. However, the Ti/Al and Si/Al ratios in oil shale are slightly higher than those in the mudstone of both members. It implies that the relatively low detrital input minimizes the effect of organic matter (OM) dilution. Conversely, it may bring the nutrient (e.g. P, N) supply to aquatic organisms (e.g. algae), leading to an increased bioproductivity and promoting the enrichment of OM.

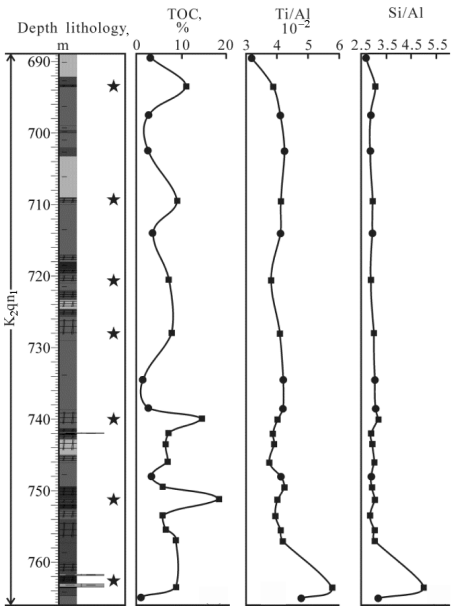

Fig. 12. Proxies for detrital matter input of K_2qn_1 including Ti/Al and Si/Al. TOC contents are shown for comparison.

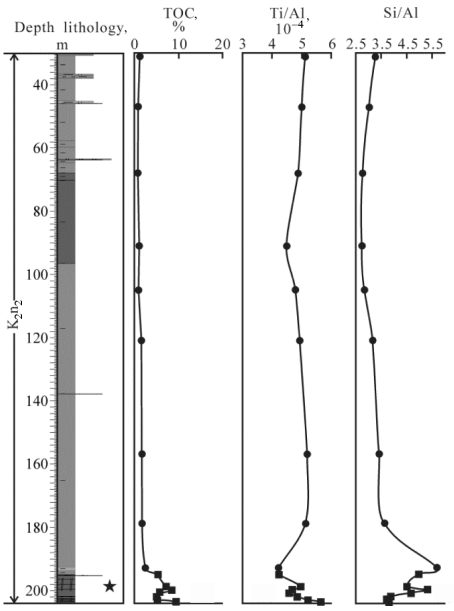

Fig. 13. Proxies for detrital matter input of K_2n_2 including Ti/Al and Si/Al. TOC contents are shown for comparison.

4.6. Paleosalinity

Strontium (Sr) and barium (Ba) are elements with different geochemical behavior in various sedimentary environments. The Sr/Ba ratio is widely regarded as an empirical indicator of paleosalinity [37]. Generally, a low Sr/Ba ratio (< 0.5) reflects fresh water, a moderate Sr/Ba (0.5–1) indicates

brackish water, and a high Sr/Ba ratio reflects saline water [37]. The calcium (Ca)/(Ca + Fe) ratio has also been used as an indicator of paleosalinity [38].

The relatively high Sr/Ba (avg. 0.87) and Ca/(Ca+Fe) (avg. 0.43) ratios imply brackish water during the deposition of K_2qn_1 (Fig. 14, Table), while the low Sr/Ba (avg. 0.40) and Ca/(Ca + Fe) (avg. 0.21) reflect fresh water in K_2n_2 (Fig. 15, Table).

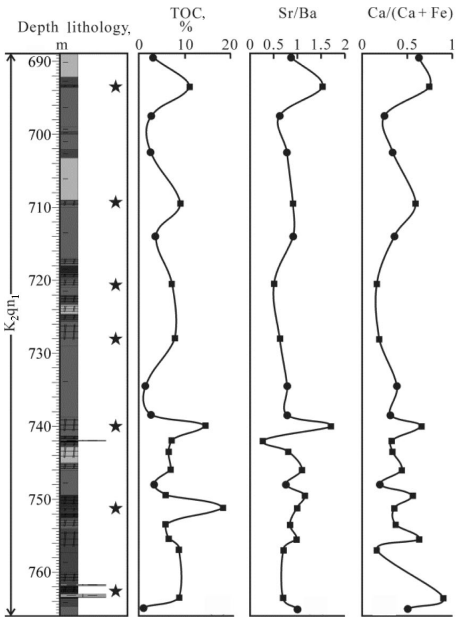

Fig. 14. Proxies for paleosalinity of K_2qn_1 including Sr/Ba and Ca/(Ca + Fe). TOC contents are shown for comparison.

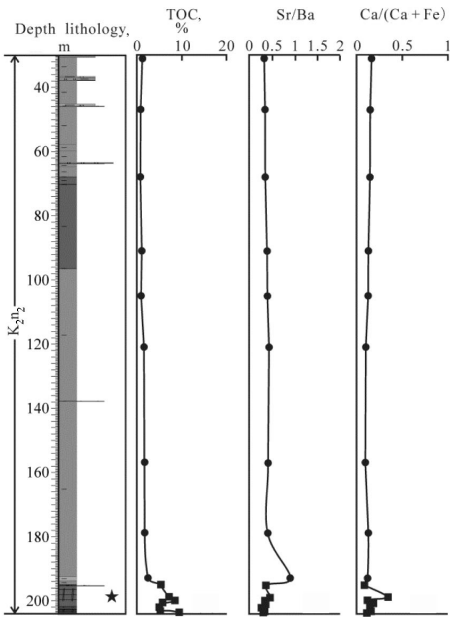

Fig. 15. Proxies for paleosalinity of K_2n_2 including Sr/Ba and Ca/(Ca + Fe). TOC contents are shown for comparison.

4.7. Bioproductivity

As phosphorus (P) is the limiting nutrient in lakes, its content is linked to primary productivity [13]. Uranium (U) is less influenced by the "grain size effect" in the reducing conditions, so it can also be used as a proxy for primary productivity [39].

The P (avg. 0.112%) and U (avg. 6.32 μg/g) contents in the K_2qn_1 oil shale are higher than those in mudstone (P avg. 0.073%; U avg. 5.13 μg/g) (Fig. 16, Table). In contrast, relatively low concentrations of P and U are present in the K_2n_2 oil shale (P avg. 0.072%; U avg. 5.92 μg/g) and mudstone (P avg. 0.069%; U avg. 3 μg/g) (Fig. 17, Table). It reflects the increased nutrient input, leading to an increased biological productivity.

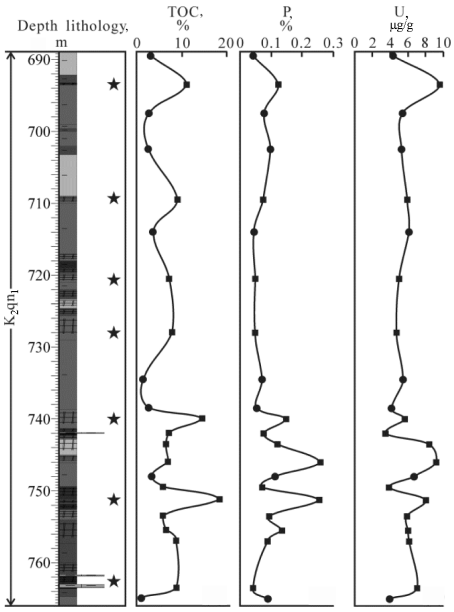

Fig. 16. Proxies for bioproductivity of K_2qn_1 including P and U contents. TOC contents are shown for comparison.

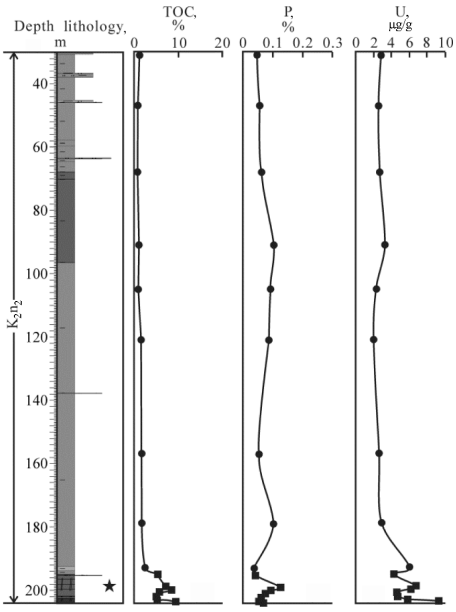

Fig. 17. Proxies for bioproductivity of K_2n_2 including P and U contents. TOC contents are shown for comparison.

4.8. Origin of organic matter

Oil shale organic matter is subdivided into three types: type I OM (aquatic OM, such as algae), type II OM (mixed type) and type III OM (terrigenous OM, such as higher plants) [14, 15]. The HI vs Rock-Eval T_{max} and S_2 vs TOC diagrams have been applied to determine the type of OM [40]. The HI vs oxygen index (OI) has not been used because of unreliable OI values.

Most of the K_2qn_1 oil shale samples have type I kerogen, a few samples with type II kerogen may have been influenced by carbonate nodule or layers (Fig. 18a–b). However, the result for mudstone is not representative due to the low number of samples studied (n = 8). According to a previous study with n = 64 [15], the OM type of K_2qn_1 mudstone samples is mainly II, a few samples having type I kerogen. This proves that aquatic organisms were the main primary producers of OM during the deposition of oil shale, whereas the mixture of aquatic and terrigenous OM was the dominant primary producer of mudstone.

It has been shown that there are distinctive differences in OM type between the oil shale and mudstone within K_2n_2. According to the plots of HI vs T_{max} and S_2 vs TOC (Fig. 18c–d), the oil shale samples have mainly type I kerogen, while most mudstone samples contain type III kerogen and a few have type II kerogen. It suggests that aquatic organisms were the major primary producers of OM during the accumulation of oil shale, whereas terrigenous plants mainly contributed to the OM of mudstone.

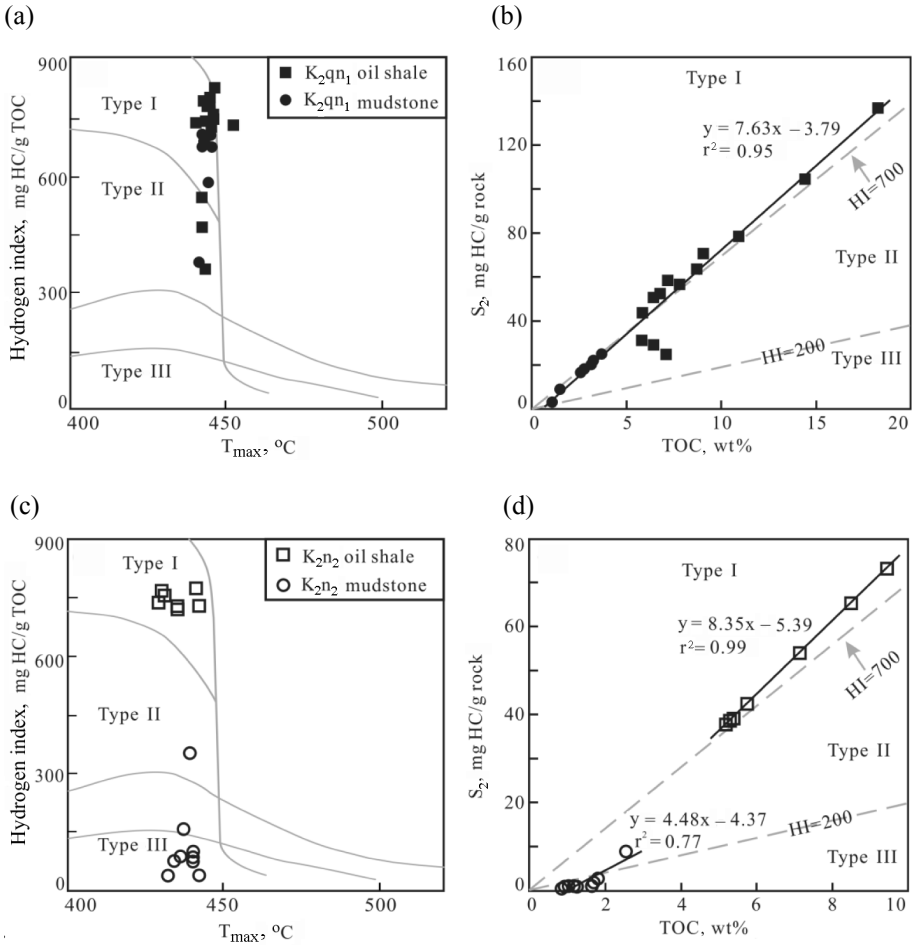

Fig. 18. Plots of T_{max} vs HI and S_2 vs TOC outlining kerogen type and source potential sediments from K_2qn_1 ((a), (b)) and K_2n_2 ((c), (d)).

5. Factors influencing organic matter enrichment

OM enrichment in sediments enhanced by bioproductivity, increased preservation of OM and decreased dilution by detrital minerals [4, 6] can be expressed by the following relation: OM enrichment = (production-destruction)/dilution. Generally, the ratio of OM to TOC is 1.22–1.33 [41], therefore TOC can reveal the OM content in sediments.

5.1. Factors influencing bioproductivity

The warm-humid paleoclimate is beneficial for mineral nutrient supply and phytoplankton growth [4], increasing bioproductivity. Based on the Sr/Cu ratio, K_2qn_1 was deposited in a warm-humid paleoclimate, whereas the

paleoclimate became warm semi-humid during the deposition of K_2n_2. This interpretation is confirmed by sporo-pollen assemblages and oxygen isotope data [24, 25]. Thus, the higher OM content in K_2qn_1 may be related to the highly warm-humid paleoclimate.

Moreover, blooms of aquatic organisms can increase bioproductivity, during the period of lake level rises [15]. The P content in the K_2qn_1 oil shale is slightly higher than that in the K_2n_2 oil shale, which may be indicative of a higher eutrophicity of the lake during the deposition of K_2qn_1. Therefore, the increased lake eutrophication during the deposition of K_2qn_1 may have been governed by the highly warm-humid paleoclimate.

Furthermore, the origin of OM affects bioproductivity [14]. The K_2qn_1 and K_2n_2 samples are immature to marginally mature, and with increasing HI, the OM type gradually transformed from III to I, i.e. from terrigenous OM to aquatic OM. The plot of TOC vs HI shows the K_2qn_1 samples to lack the corresponding correlation (Fig. 19a). In contrast, the TOC-HI plot for the K_2n_2 samples illustrates a strong positive correlation (r^2 = 0.94) (Fig. 19b). It indicates that OM enrichment within K_2qn_1 was less influenced by its origin unlike K_2n_2, where OM origin governed its enrichment, while with the rising proportion of aquatic organisms, the OM abundance increased.

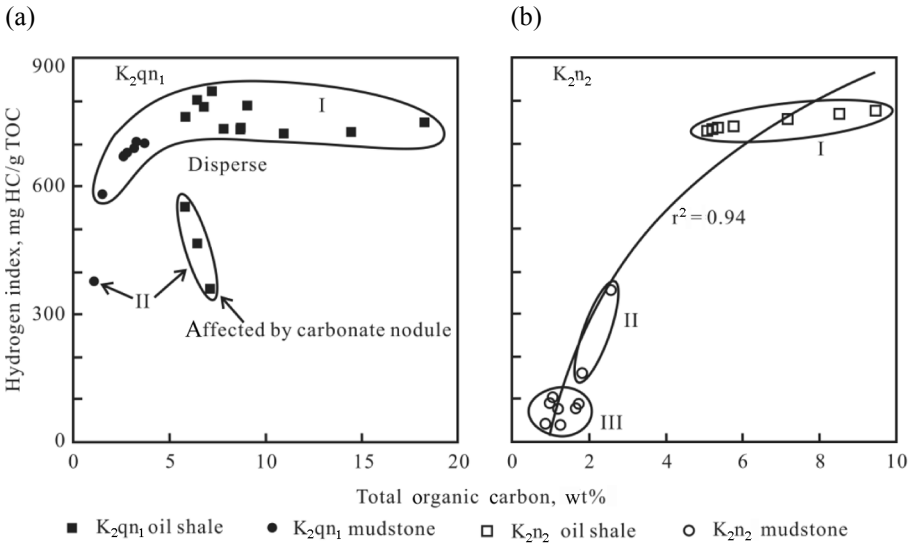

Fig. 19. Plot of TOC vs HI of (a) K_2qn_1 and (b) K_2n_2.

5.2. Factors influencing preservation conditions

The preservation of OM is a complex physical and chemical process, and multiple factors have been put forward as controlling factors of this process in sediments [3].

According to the ratios of Sr/Ba and Ca/(Ca + Fe), the paleosalinity in K_2qn_1 was brackish-saline and the lake water salinity stratification was strong, whereas K_2n_2 was deposited in fresh-brackish water and had a weak water salinity stratification. The stable dysoxic conditions in K_2qn_1 are revealed by C-S-Fe relationships, HI, V/Cr ratio, $EF_{(Mo/Al)}$ and Ce-anomaly. In contrast, fluctuant redox conditions prevailed during the deposition of K_2n_2, while in the lower part of the Songliao Basin (oil shale) the conditions were dysoxic and in its upper part (mudstone) marginally oxic.

The results demonstrate that the highly warm-humid paleoclimate related to lake level rises was responsible for the strong water salinity stratification and reducing conditions (dysoxic or anoxic). Another reason for the high water salinity within K_2qn_1 could have been marine transgression events during the early deposition of the Qingshankou Formation [42], which supposition is supported by the evidence of the presence of marine organisms (bivalve), fossil fish and foraminifera [43–45].

In the diagrams of paleosalinity (Sr/Ba) vs paleo-redox conditions (V/Cr), the K_2qn_1 samples reflect stable redox conditions and fluctuant water salinity (Fig. 20a), while the water salinity of oil shale was generally higher. In contrast, fluctuant redox conditions and stable water salinity are revealed by the K_2n_2 samples (Fig. 20b), whereas oil shale mainly accumulated in highly reducing conditions (dysoxic).

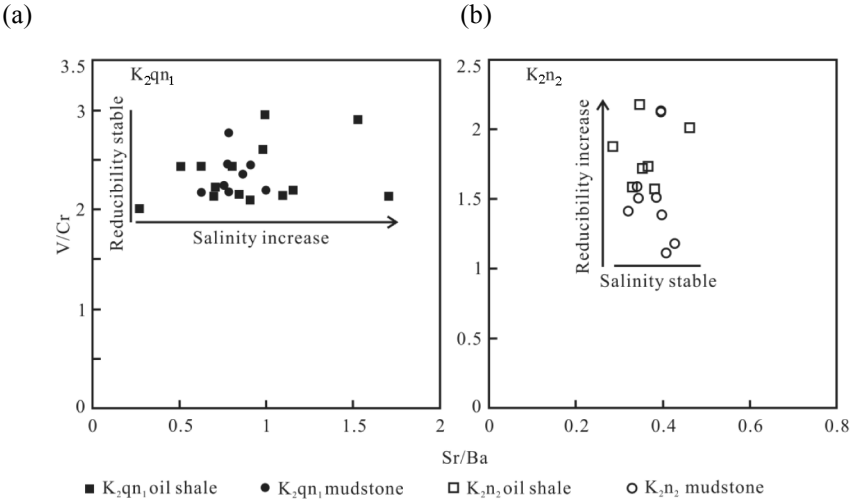

Fig. 20. Plot of Sr/Ba vs V/Cr of (a) K_2qn_1 and (b) K_2n_2.

5.3. Factors influencing dilution

The input of detrital matter is not only responsible for the dilution of OM, but is also associated with the increased nutrient supply leading to blooms of aquatic organisms [6]. The Al_2O_3/TiO_2 ratios of Qingshankou and Nenjiang Formations demonstrate that there is a constant sediment source region of

intermediate to felsic igneous rocks (see 4.2), although this ratio in K_2qn_1 (avg. 28.0) is slightly higher than that in K_2n_2 (avg. 23.5) (Table).

K_2qn_1 and K_2n_2 were deposited during the major lacustrine transgression (Fig. 1). Thus, the decrease of detrital matter input over time should have been expected. The observed Ti/Al and Si/Al trends in K_2qn_1 agree with this assumption (Fig. 12). However, the Ti/Al and Si/Al trends in K_2n_2 do not support this supposition, the two ratios in the upper part of K_2n_2 are slightly higher than those in its lower part (Fig. 13). That may have been caused by the reduced lake area and the tectonic uplift of the eastern basin flank during the late deposition of K_2n_2, which promoted mineral matter input from the eastern provenance and resulted in detrital mineral matter input, including land plants, and dilution of OM.

6. Summary and conclusions

Two oil shale layers are present in the Upper Cretaceous Qingshankou and Nenjiang Formations of the Songliao Basin, NE China. According to bulk geochemical data, the K_2qn_1 oil shale samples with high TOC contents (avg. 8.79 wt%) are dominated by type I kerogen (aquatic organisms), while the TOC contents of mudstone samples are low (avg. 2.56 wt%) and kerogen type is II (mixed type). At the same time, the K_2n_2 oil shale samples with medium TOC contents (avg. 6.66 wt%) are also dominated by type I kerogen (aquatic organisms), while the TOC contents of mudstone samples are low (avg. 1.44 wt%) and kerogen type is III (terrigenous plants).

The Sr/Cu ratio indicates that K_2qn_1 was deposited in a warm-humid paleoclimate, whereas the paleoclimate became warm semi-humid during the deposition of K_2n_2, which is confirmed by the sporo-pollen assemblages and oxygen isotope data. According to the C-S-Fe relationships, HI, $EF_{(Mo/Al)}$, V/Cr, Ce-anomaly, and Sr/Ba and Ca/(Ca + Fe) ratios, strong water salinity stratification and dysoxic conditions were prevailing during the deposition of K_2qn_1 oil shale. In contrast, the K_2n_2 oil shale was deposited in weak water salinity stratification and partially oxic conditions. The high bioproductivity and low detrital matter input within K_2qn_1, and the medium bioproductivity and detrital matter input within K_2n_2 are confirmed by Ti/Al and Si/Al ratios and P and U contents.

The comprehensive study of the bioproductivity, preservation and dilution of OM demonstrates that there are significant differences in OM enrichment models between K_2qn_1 (Fig. 21a) and K_2n_2 (Fig. 21b) in the Songliao Basin. In summary, high bioproductivity and strong water salinity stratification were responsible for OM enrichment in K_2qn_1, whereas the origin of OM and dysoxic conditions were the major controlling factors of OM enrichment in K_2n_2.

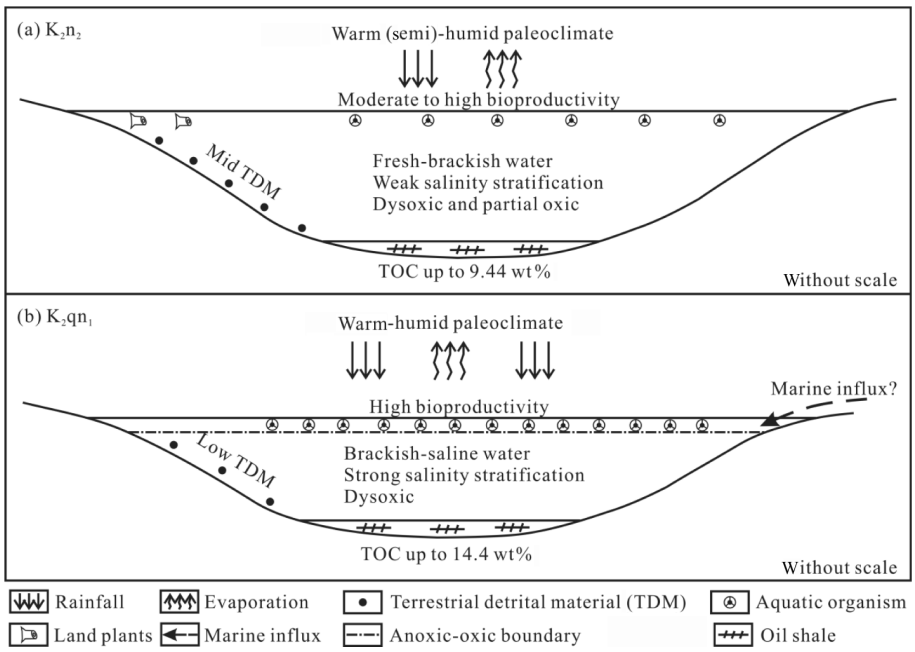

Fig. 21. The OM enrichment model of (a) K_2qn_1 and (b) K_2n_2 in the Songliao Basin.

Acknowledgements

We appreciate the support from the Opening Foundation of Key Laboratory for Oil Shale and Paragenetic Energy Minerals, Jilin Province, China. The research project was financially supported by the China Geological Survey (1212011220800-02, 1211302108025-5-1).

REFERENCES

1. Mayer, L. M. Surface area control of organic carbon accumulation in continental shelf sediments. *Geochim. Cosmochim. Ac.*, 1994, **58**(4), 1271–1284.
2. Kennedy, M. J., Pevear, D. R., Hill, R. J. Mineral surface control of organic carbon in black shale. *Science*, 2002, **295**(5555), 657–660.
3. Zonneveld, K. A. F., Versteegh, G. J. M., Kasten, S., Eglinton, T. I., Emeis, K.-C., Huguet, C., Koch, B. P., de Lange, G. J., de Leeuw, J. W., Middleburg. J. J., Mollenhauer, G., Prahl, F. G., Rethemeyer, J., Wakeham, S. G. Selective preservation of organic matter in marine environments; processes and impact on the sedimentary record. *Biogeosciences*, 2010, **7**(2), 483–511.
4. Talbot, M. R. The origins of lacustrine oil source rocks: evidence from the lakes of tropical Africa. In: *Lacustrine Petroleum Source Rocks* (Fleet, A. J., Kelts, K., Talbot, M. R., eds.). Geological Society, London, 1988, **40**, 29–43.
5. Bohacs, K. M. Source quality variations tied to sequence development in the Monterey and associated formations, southwestern California. In: *Source Rocks*

in a Sequence Stratigraphic Framework (Katz, B. J., Pratt, L. M., eds.). AAPG Studies in Geology, 1993, **37**, 177–204.
6. Bohacs, K. M., Carroll, A. R., Neal, J. E., Mankiewicz, P. J. Lake-basin type, source potential, and hydrocarbon character: an integrated sequence-stratigraphic-geochemical framework. In: *Lake Basins through Space and Time* (Gierlowski-Kordesch, E. H., Kelts, K. R., eds.). AAPG Studies in Geology, 2000, **46**, 3–34.
7. Pedersen, T. F., Calvert, S. E. Anoxia vs. productivity: what controls the formation of organic-carbon-rich sediments and sedimentary rocks? *AAPG Bull.*, 1990, **74**(4), 454–466.
8. Caplan, M. L., Bustin, R. M. Palaeoceanographic controls on geochemical characteristics of organic-rich Exshaw mudrocks: role of enhanced primary production. *Org. Geochem.*, 1998, **30**(2–3), 161–188.
9. Katz, B. J. Controlling factors on source rock development – a review of productivity, preservation, and sedimentation rate. In: *The Deposition of Organic-Carbon-Rich Sediments: Models, Mechanisms, and Consequences* (Harris, N. B., ed.). SEPM Special Publication, 2005, **82**, 7–16.
10. Demaison, G. J., Moore, G. T. Anoxic environments and oil source bed genesis. *AAPG Bull.*, 1980, **64**(8), 1179–1209.
11. Tyson, R. V. The "productivity versus preservation" controversy: cause, flaws, and resolution. In: *The Deposition of Organic-Carbon-Rich Sediments: Models, Mechanisms, and Consequences* (Harris, N. B., ed.). SEPM Special Publication, 2005, **82**, 17–33.
12. Murphy, A. E., Sageman, B. B., Hollander, D. J., Lyons, T. W., Brett, C. E. Black shale deposition and faunal overturn in the Devonian Appalachian Basin: clastic starvation, seasonal water-column mixing, and efficient biolimiting nutrient recycling. *Paleoceanography*, 2000, **15**(3), 280–291.
13. Sageman, B. B., Murphy, A. E., Werne, J. P., Ver Straeten, C. A., Hollander, D. J., Lyons, T. W. A tale of shales: the relative roles of production, decomposition, and dilution in the accumulation of organic-rich strata, Middle–Upper Devonian, Appalachian basin. *Chem. Geol.*, 2003, **195**, 229–273.
14. Jia, J. L., Bechtel, A., Liu, Z. J., Strobl, S. A. I., Sun, P. C., Sachsenhofer, R. F. Oil shale formation in the Upper Cretaceous Nenjiang Formation of the Songliao Basin (NE China): Implications from organic and inorganic geochemical analyses. *Int. J. Coal Geol.*, 2013, **113**, 11–26.
15. Jia, J. L., Liu, Z. J., Bechtel, A., Strobl, S. A. I., Sun, P. C. Tectonic and climate control of oil shale deposition in the Upper Cretaceous Qingshankou Formation (Songliao Basin, NE China). *Int. J. Earth Sci.*, 2013, **102**, 1717–1734.
16. Bechtel, A., Jia, J. L., Strobl, S. A. I., Sachsenhofer, R. F., Liu, Z. J., Gratzer, R., Püttmann, W. Palaeoenvironmental conditions during deposition of the Upper Cretaceous oil shale sequences in the Songliao Basin (NE China): implications from geochemical analysis. *Org. Geochem.*, 2012, **46**, 76–95.
17. Jia, J. L., Liu, Z. J., Meng, Q. T., Liu, R., Sun, P. C., Chen, Y. C. Quantitative evaluation of oil shale based on well log and 3-D seismic technique in the Songliao Basin, Northeast China. *Oil Shale*, 2012, **29**(2), 128–150.
18. Feng, Z. Q., Jia, C. Z., Xie, X. N., Zhang, S., Feng, Z. H., Timothy, A. C. Tectonostratigraphic units and stratigraphic sequences of the nonmarine Songliao basin, northeast China. *Basin Res.*, 2010, **22**(1), 79–95.
19. Liu, Z. J., Sun, P. C., Jia, J. L., Meng, Q. T. Distinguishing features and their genetic interpretation of stratigraphic sequences in continental deep water

setting: A case from Qingshankou Formation in Songliao Basin. *Earth Science Frontiers*, 2011, **18**(4), 171–180 (in Chinese, summary in English).
20. Nali, M., Caccialanza, G., Ghiselli, C., Chiaramonte, M. A. T_{max} of asphaltenes: a parameter for oil maturity assessment. *Org. Geochem.*, 2000, **31**(12), 1325–1332.
21. Hayashi, K. I., Fujisawa, H., Holland, H. D., Ohmoto, H. Geochemistry of 1.9 Ga sedimentary rocks from northeastern Labrador, Canada. *Geochim. Cosmochim. Ac.*, 1997, **61**(19), 4115–4137.
22. Ross, D. J. K., Bustin, R. M. Investigating the use of sedimentary geochemical proxies for paleoenvironment interpretation of thermally mature organic-rich strata: examples from the Devonian-Mississippian shales, Western Canadian Sedimentary Basin. *Chemi. Geol.*, 2009, **260**, 1–19.
23. Meng, Q. T., Liu, Z. J., Bruch, A. A., Liu, R., Hu, F. Palaeoclimatic evolution during Eocene and its influence on oil shale mineralisation, Fushun basin, China. *J. Asian Earth Sci.*, 2012, **45**, 95–105.
24. Huang, Q. H., Zheng, Y. L., Yang, M. J., Li, X. J., Han, M. X., Chen, C. R. On Cretaceous paleoclimate in the Songliao basin. *Acta Micropalaeontologica Sinica*, 1999, **16**(1), 95–103 (in Chinese, summary in English).
25. Wang, C. S., Feng, Z. Q., Zhang, L. M., Huang, Y. J., Cao, K., Wang, P. J., Zhao, B. Cretaceous paleogeography and paleoclimate and the setting of SKI borehole sites in Songliao Basin, northeast China. *Palaeogeogr. Palaeocl.*, 2013, **385**, 17–30.
26. Berner, R. A., Raiswell, R. Burial of organic carbon and pyrite sulfur in sediments over Phanerozoic time: A new theory. *Geochim. Cosmochim. Ac.*, 1983, **47**(5), 855–862.
27. Raiswell, R., Buckley, F., Berber, R. A., Anderson, T. F. Degree of pyritization of iron as a paleoenvironmental indicator of bottom-water oxygenation. *J. Sediment. Petrol.*, 1988, **58**(5), 812–819.
28. Dean, W. E., Arthur, M. A. Iron–sulfur–carbon relationships in organic-carbon-rich sequences. I: Cretaceous Western Interior Seaway. *Am. J. Sci.*, 1989, **289**, 708–743.
29. Arthur, M. A., Sageman, B. B. Marine black shales: depositional mechanisms and environments of ancient deposits. *Ann. Rev. Earth Pl. Sc.*, 1994, **22**, 499–551.
30. Talbot, M. R., Livingstone, D. A. Hydrogen index and carbon isotopes of lacustrine organic matter as lake level indicators. *Palaeogeogr. Palaeocl.*, 1989, **70**(1–3), 121–137.
31. Wedepohl, K. H. Environmental influences on the chemical composition of shales and clays. In: *Physics and Chemistry of the Earth, vol. 8* (Ahrens, L. H., Press, F., Runcorn, S. K., Urey, H. C., eds.). Pergamon, Oxford, 1971, 305–333.
32. Lyons, T. W., Werne, J. P., Hollander, D. J., Murray, R. W. Contrasting sulfur geochemistry and Fe/Al and Mo/Al ratios across the last oxic-to-anoxic transition in the Cariaco Basin, Venezuela. *Chem. Geol.*, 2003, **195**(1–4), 131–157.
33. Algeo, T. J., Maynard, J. B. Trace element behavior and redox facies of core shales of Upper Pennsylvanian Kansas-type cyclotherms. *Chem. Geol.*, 2004, **206**, 289–318.
34. Jones, B., Manning, D. A. C. Comparison of geochemical indices used for the interpretation of palaeoredox conditions in ancient mudstones. *Chem. Geol.*, 1994, **111**(1–4), 111–129.

35. Wilde, P., Quinby-Hunt, M. S., Erdtmann, B. D. The whole-rock cerium anomaly: a potential indicator of eustatic sea-level changes in shales of the anoxic facies. *Sediment. Geol.*, 1996, **101**(1–2), 43–53.
36. Calvert, S. E., Bustin, R. M., Ingall, E. D. Influence of water column anoxia and sediment supply on the burial and preservation of organic carbon in marine shales. *Geochim. Cosmochim. Ac.*, 1996, **60**(9), 1577–1593.
37. Wang, A. H. Discriminant effect of sedimentary environment by the Sr/Ba ratio of different existing forms. *Acta Sedimentologica Sinica*, 1996, **14**(4), 168–173 (in Chinese, summary in English).
38. Zhang, M. M., Liu, Z. J., Xu, S. C., Sun, P. C., Hu, X. F. Element response to the ancient lake information and its evolution history of argillaceous source rocks in the Lucaogou Formation in Sangonghe area of southern margin of Junggar Basin. *J. Earth Sci.*, 2013, **24**(6), 987–996.
39. Chase, Z., Anderson, R. F., Fleisher, M. Q. Evidence from authigenic uranium for increased productivity of the glacial subantarctic ocean. *Paleoceanography*, 2001, **16**(5), 468–478.
40. Langford, F. F., Blanc-Valleron, M.-M. Interpreting Rock-Eval pyrolysis data using graphs of pyrolizable hydrocarbons vs. total organic carbon. *AAPG Bull.*, 1990, **74**(6), 799–804.
41. Hunt, J. M. *Petroleum Geochemistry and Geology*, 2nd ed. W. H. Freeman and Company, San Francisco, 1995, 491–524.
42. Huang, Y. J., Yang, G. S., Gu, J., Wang, P. K., Huang, Q. H., Feng, Z. H., Feng, L. J. Marine incursion events in the Late Cretaceous Songliao Basin: Constraints from sulfur geochemistry records. *Palaeogeogr. Palaeocl.*, 2013, **385**, 152–161.
43. Gu, Z. W., Huang, B. Y., Chen, C. Z. *Fossil Lamellibranchiata of China*. Science Press, Beijing, 1976, 80–110 (in Chinese).
44. Zhang, M. M., Zhou, J. J. On the fossil fishes in Mesozoic and Cenozoic oil-bearing strata from East China and their sedimentary environment. *Vertebrata Palasiatica*, 1978, **16**, 229–237 (in Chinese, summary in English).
45. Xi, D. P., Wan, X. Q., Feng, Z. Q., Li, S., Feng, Z. H., Jia, J. Z., Jing, X., Si, W. M. Discovery of Late Cretaceous foraminifera in the Songliao Basin: evidence from SK-1 and implications for identifying seawater incursions. *Chinese Science Bulletin*, 2011, **56**(3), 253–256 (in Chinese, summary in English).

Presented by K. Kirsimäe
Received March 19, 2015